Evidence for renoxification in the tropical marine boundary layer

Chris Reed[1†], Mathew J. Evans[1,2], Leigh R. Crilley[3], William J. Bloss[3], Tomás Sherwen[1], Katie A. Read[1,2], James D. Lee[1,2] and Lucy J. Carpenter[1]

[1] Wolfson Atmospheric Chemistry Laboratories (WACL), Department of Chemistry, University of York, Heslington, York, YO10 5DD, United Kingdom

[2] National Centre for Atmospheric Science (NCAS), University of York, Heslington, York, YO10 5DD, United Kingdom

[3] School of Geography, Earth and Environmental Sciences, University of Birmingham, Edgbaston, Birmingham, B15 2TT, United Kingdom

Corresponding author: Chris Reed (chris.paul.reed@gmail.com)

†Now at Facility for Airborne Atmospheric Measurements (FAAM), Building 146, Cranfield University, Cranfield, MK43 0AL, United Kingdom

Abstract

We present two years of NO_x observations from the Cape Verde Atmospheric Observatory located in the tropical Atlantic boundary layer. We find NO_x mixing ratios peak around solar noon (at 20-30 pptV depending on season), which is counter to box model simulations that show a midday minimum due to OH conversion of NO_2 to HNO_3. Production of NO_x via decomposition of organic nitrogen species and the photolysis of HNO_3 appear insufficient to provide the observed noon-time maximum. A rapid photolysis of nitrate aerosol to produce HONO and NO_2, however, is able to simulate the observed diurnal cycle. This would make it the dominant source of NO_x at this remote marine boundary layer site overturning the previous paradigm of transport of organic nitrogen species such as PAN being the dominant source. We show that observed mixing ratios (Nov-Dec 2015) of HONO at Cape Verde (~3.5 pptV peak at solar noon) are consistent with this route for NO_x production. Reactions between the nitrate radical and halogen hydroxides which have been postulated in the literature appear to improve the box model simulation of NO_x. This rapid conversion of aerosol phase nitrate to NO_x changes our perspective of the NO_x cycling chemistry in the tropical marine boundary layer, suggesting a more chemically complex environment than previously thought.

1 Introduction

The chemical environment in the remote marine boundary layer (MBL) is characterized by very low concentrations of nitrogen oxides (NO_x = NO + NO_2) i.e. 10 to <100 pptV (Carsey et al., 1997; Lee et al., 2009; Monks et al., 1998), high concentrations of water vapour and the presence of inorganic halogen compounds, resulting in net daytime ozone (O_3) destruction (Dickerson et al., 1999; Read et al., 2008; Sherwen et al., 2016; Vogt et al., 1999). This MBL loss of ozone plays an important role in determining the global budget of ozone and the overall oxidizing capacity of the region. Understanding the concentrations of NO_x in these environments is thus important for determining the global ozone budget, alongside wider atmospheric chemical impacts.

NO_x in the remote MBL has been attributed to a) long range transport and decomposition of species such as peroxy acetyl nitrates (PAN), organic nitrates, or HNO_3 (Moxim et al., 1996) b) shipping emissions (Beirle et al., 2004) c) a direct ocean source (Neu et al., 2008) and d) its direct atmospheric transport (Moxim et al., 1996). However, more recently the possibility of 'renoxification' by rapid nitrate photolysis on a variety of surfaces has garnered attention. Photolytic rate enhancements have been reported on aerosol nitrate (Ndour et al., 2009; Ye et al., 2016b), urban grime (Baergen and Donaldson, 2013, 2016), natural and artificial surfaces (Ye et al., 2016a), and in laboratory prepared organic films and aqueous solutions (Handley et al., 2007; Scharko et al., 2014; Zhou et al., 2003).

The oxidation of NO_2 to HNO_3 by OH is the predominant sink for NO_x in the remote-MBL. NO_x can also be converted into aerosol phase nitrate via the hydrolysis of N_2O_5 (R2) (Evans, 2005) but this is a slow gas phase process in these low NO_x environments. NO_x can be returned through HNO_3 photolysis (R3) or reaction with OH (R4) but in general these processes are again slow in the gas phase and so HNO_3 can deposit to the surface, be washed out by rain, or taken up by aerosol (R5).

$$NO_2 + OH + M \rightarrow HNO_3 + M \qquad \text{(R1)}$$

$$N_2O_5 + H_2O_{(aer)} \rightarrow 2HNO_{3(aer)} \qquad \text{(R2)}$$

$$HNO_3 + hv \rightarrow OH + NO_2 \quad (R3)$$

$$HNO_3 + OH \rightarrow NO_3 + H_2O \quad (R4)$$

$$HNO_{3(g)} + aerosol \rightarrow HNO_{3(aer)} \quad (R5)$$

More recently the production and subsequent hydrolysis of halogen nitrates ($IONO_2$, $BrONO_2$, $ClONO_2$) have been suggested to be a potentially important sink for NO_x in the marine boundary layer (Keene et al., 2007, 2009; Lawler et al., 2009; Pszenny et al., 2004; Sander et al., 1999)

In this paper we investigate the budget of NO_x in the remote MBL using observations of NO_x and HONO collected at the Cape Verde Atmospheric Observatory during 2014 and 2015. We use a 0-D model of NO_x, HO_x, halogen, and VOC chemistry to interpret these observations and investigate the role that different NO_x source and sink terms play.

2 Methodology

The Cape Verde Atmospheric Observatory (CVO), a WMO Global Atmospheric Watch (GAW) station, is located in the tropical North Atlantic (16.864, -24.868) on the island of São Vincente and is exposed to air travelling from the North East in the trade winds (Carpenter et al., 2010). In general, the air reaching the station has travelled many days over the ocean since exposure to anthropogenic emissions, thus the station is considered representative of the remote marine boundary layer (Read et al., 2008). A large range of compounds are measured at the CVO (Carpenter et al., 2010), but we focus here on the NO and NO_2 continuous measurements, alongside HONO measurements that were made for 10 days in Winter 2015.

2.1 NO and NO_2

NO and NO_2 are measured by NO chemiluminescence (Drummond et al., 1985) coupled to photolytic NO_2 conversion by selective photolysis at 385-395 nm as described by (Lee et al., 2009; Pollack et al., 2011; Reed et al., 2016a, 2016b; Ryerson et al., 2000). A single photomultiplier detector switches between 1 minute of chemiluminescent zero, 2 minutes of NO, and 2 minutes of NO_x measurement.

Air is sampled from a common 40 mm glass manifold (QVF) which draws ambient air from a height of 10m above ground level. The manifold is downward facing into the prevailing wind at the inlet and fitted with a hood. The manifold is shielded from sunlight outside, and thermostated within the lab to 30°C to prevent condensation. Air is drawn down by centrifugal pump at ~ 750 L/min^{-1} resulting in a sample flow speed of 10 m/s^{-1} and a residence time to the NO_x instrument of 2.3 seconds. Humidity and aerosol are reduced by two dead-end traps at the lowest points of the manifold inside and outside the lab which are drained off regularly. Manifold sample flow, humidity and temperature are recorded and logged continuously.

Air is sampled a 90° to the manifold flow through ¼ inch PFA tubing at 1 standard L per minute, being filtered through a 47mm, 0.22 μm mesh filter before entering the NO_x analyser.

The humidity of the sample gas is further reduced by a Nafion dryer (PD-50T-12-MKR, Permapure), fed by a constant sheath flow of zero air (PAG 003, Eco Physics AG) which is also filtered through a Sofnofil (Molecular Products) and activated carbon (Sigma Aldrich) trap. This reduces sample humidity variability which affected NO sensitivity through chemiluminescent quenching (Clough and Thrush, 1967) where sample humidity can vary from 60 to 90% (Carpenter et al., 2010). Calibration for NO sensitivity and NO_2 converter efficiency occurs every 73 hours by standard addition to ambient air as described by Lee et al., (2009); in this way correction for humidity affecting sensitivity, and O_3 affecting NO_2 conversion efficiency are unnecessary. Sensitivity drift between calibration is <2%, within the overall uncertainty of the measurement. Zero air is also used to determine the NO_2 artifact signal which can arise when NO_x free air is illuminated at UV wavelengths due to photolysis of HNO_3 etc., adsorbed on the walls of the photolysis cell (Nakamura et al., 2003; Pollack et al., 2011; Ryerson et al., 2000). NO artifact correction is made by assuming it is equivalent to a stable night-time NO value in remote regions (Lee et al., 2009), away from any emission source, where NO should be zero in the presence of O_3. Reed et al., (2016b) showed that thermal interferences in NO_2 using this technique may cause a bias in cold or temperate remote regions, but that in warm regions, such as Cape Verde, the effect is negligible. Photolytic interferences such as $BrONO_2$ and HONO, and inlet effects may also alter the retrieved NO or NO_2 (Reed et al., 2016a, 2016b). These effects are considered to be sufficiently small that the concentrations of NO and NO_2 can be determined

within an accuracy of 5% and 5.9% respectively (Reed et al., 2016a, 2016b) at the (very low) levels present at CVO. The instrument having a zero count rate of ~ 1700 Hz with 1 σ standard deviation of that signal ~ 50 Hz this gives a precision of 7.2 pptV for 1 second data with typical sensitivity over the measurement period of 6.9 cps/pptV. The resultant limits of detection for NO and NO_2 being 0.30 and 0.35 pptV when averaged over an hour.

2.2 HONO

Between 24th November and 3rd December 2015 a Long Path Absorption Photometer (LOPAP) (Heland et al., 2001) was employed at CVO to provide an *in-situ* measurement of nitrous acid. The LOPAP has its own thermostated inlet system with reactive HONO stripping to minimise losses so does not sample from the main lab manifold. The LOPAP inlet was installed on the roof of a container lab ~ 2.5 m above ground level, unobstructed from the prevailing wind. Calibration and operation of the LOPAP was carried out in line with the standard procedures described by Kleffmann and Wiesen, (2008). Specifically at CVO, the sampling conditions were set in order to maximise the sensitivity of the LOPAP, using a gas sampling flow rate of 2 standard L per minute. A two point calibration was performed using a standard solution of nitrite (NO_2^-) at concentrations of 0.8 and 10 µg L^{-1}. To account for instrument drift, baseline measurements using an overflow of high-purity N_2 were performed at regular intervals (8 hours). The detection limit of the LOPAP (2σ) was calculated by the variability during a typical baseline measurement under N_2 and was found to be 0.2 pptV. The relative error of the LOPAP was conservatively set to 10% of the measured concentration.

2.3 Box Model

We use the Dynamically Simple Model of Atmospheric Chemical Complexity (DSMACC) box model (Emmerson and Evans, 2009) to interpret the observed NO_x measurements. We focus on the summer season (June, July, and August) as this has the largest data coverage (N=153) and is out of dust season which extends through winter and spring (Carpenter et al., 2010; Fomba et al., 2014; Ridley et al., 2014) and coincides with the lowest NO_y mixing ratios (Carpenter et al., 2010). The model is run for day 199 at 16.864°N, -024.868°W. We initialize the model with the mean observed H_2O, CO, O_3, VOCs (Carpenter et al., 2010; Read et al., 2012), 100 $\mu m^2/cm^3$

aerosol surface area (Carpenter et al., 2010). We also initialise the model with 1.5 pptV of I_2 and 2.5 pptV of Br_2 to provide ~1.5 pptV of IO and ~2.5 pptV BrO during the day, consistent with the levels measured over 9 months at the CVO during 2007 (Mahajan et al., 2010; Read et al., 2008). We use the average diurnal cycle of the measured HONO concentrations, described above. Solar radiation at this location in the tropics shows little seasonal variation, hence photolysis rates are similar in summer and autumn. This measurement period was also free of dust influence. We assume clear sky conditions for photolysis. The meteorological parameters pressure, temperature, relative humidity, and boundary layer height are set to median values reported by Carpenter et al., (2010). Boundary layer height is fixed at 713m as no overall seasonal or diel pattern is evident in boundary layer height at Cape Verde (Carpenter et al., 2010). This is expected at a site representative of the marine boundary layer, which has almost no island effects (except for very rare instances of wind outside the northwesterly sector, which are excluded). Thus, we discount any influence from boundary layer height changes on the diurnal cycles presented.

The unconstrained model is run forwards in time until a stable diurnal cycle is attained; ~ 3 days. A full description of the model chemistry is provided in the supplementary material. The base case chemistry has only gas phase sources plus gas phase and deposition sinks for NO_x as described in the supplementary material.

3 Results and discussion

3.1 Diurnal cycles in NO_x and HONO

Figure 1 shows the measured mean diurnal cycles of NO, NO_2, NO_x, and O_3 observed in each season (Meteorological Spring, Summer, Autumn, and Winter) during 2014 and 2015. Every season shows a strong diurnal cycle in NO, peaking after solar noon at around ~13:00 to 14:00. The diurnal cycle of NO_2 is much less pronounced but also exhibits weak maxima in the early afternoon. Overall this leads to a maximum in NO_x during the day. This behaviour is consistent throughout the year and air mass, though not necessarily on a “day-to-day” basis.

The observed diurnal cycle in NO_x is hard to explain with conventional chemistry. The increase in night time NO_x suggests a continuous source but the maximum around noon suggests a photolytic source. Given the predominant NO_x sink is reaction with OH to form HNO_3, it would be expected that there would be a minimum in NO_x during the day rather than a maximum. Similar observations have been reported previously (Monks et al., 1998) at the Cape Grim Baseline Air Pollution station (-40.683, 144.670), a comparably remote site in the southern hemisphere, and during the Atlantic Stratocumulus Transition Experiment (ASTEX) cruise (~29°N, 24°W) which reported similar daytime NO_x production (Carsey et al., 1997). The observed behaviour in the CVO NO_x was historically attributed to atmospheric thermal decomposition of NO_y species (Lee et al., 2009).

Figure 2 shows the average diurnal cycle at CVO of measured HONO concentrations. The data exhibits a strong daytime maximum peaking at noon local time (Solar noon ~13:20) and reaching near zero at night, indicating a photolytic source. HONO is lost through deposition, photolysis and reaction with OH, whilst night time build-up often observed (Ren et al., 2010; VandenBoer et al., 2014; Zhou et al., 2002), here HONO appears to reach a steady state concentration of ~0.65 pptV throughout the night. This pseudo steady state behaviour of nocturnal HONO has previously been reported in the polluted marine boundary layer by Wojtal et al., (2011), albeit reporting much higher HONO mixing ratios.

Daytime production of HONO is similarly hard to reconcile if its formation by the homogeneous OH + NO reaction (or other gas-phase HO_x-NO_x chemistry, e.g. Li et al., (2014)). With NO mixing ratios below 5 pptV, OH measured peaking at ~ 0.25 pptV during the RHaMBLe campaign (Carpenter et al., 2010; Whalley et al., 2010) and a maximum noontime *j*HONO of 1.2 $\times 10^{-3}$ s^{-1}, a steady state HONO mixing ratio of ~ 0.04 pptV is found ($k_{(OH + NO)} = 7.4 \times 10^{-12}$ $mol.cm^{-3}$ s^{-1}). An additional daytime source of HONO must be present to explain the observed concentrations.

Both the long-term NO_x and the short-term HONO observations made at CVO are cannot be explained with purely gas phase chemistry. Both datasets show daytime maxima indicative of a

photolytic source of NO_x and HONO, whereas gas phase chemistry would predict minima in NO_x during daytime and two orders of magnitude less HONO.

3.2 Box modelling of NO_x sources

Using the box model (section 2.3) we explore the observed diurnal variation in NO_x and understand the role of different processes. Classically, the predominant source of NO_x in remote regions is considered to be the thermal decomposition of compounds such as peroxyacetyl nitrate (PAN) which can be produced in regions of high NO_x and transported long distances (Fischer et al., 2014; Jacobi et al., 1999; Moxim et al., 1996). We consider a source of PAN which descends from the free troposphere and then thermally decomposes to NO_2 in the warm MBL. The main sink of NO_x is conversion to HNO_3, which is slightly counterbalanced by a slow conversion of HNO_3 back into NO_x through gas phase photolysis or reaction with OH. Figure 3 shows the model with a source of PAN which results in mixing ratios of 5 – 8 pptV, consistent with the few measurements made in the marine boundary layer, most notably by Jacobi et al., (1999) who measured levels from <5 to 22 pptV in the tropical Atlantic, and Lewis et al., (2007) who reported PAN mixing ratios of ~10 pptV in the remote mid-Atlantic MBL.

It is evident from the base case model results shown in Fig. 3 that the model fails to calculate the NO_x and HONO diurnal cycles. Modelled NO_x concentrations do increase during the night, consistent with the observations, but the model's minimum for NO_x occurs during the day when the observations show a maximum. The modelled and measured HONO is also shown in Fig. 3, both peaking during midday with observations reaching 3.5 pptV whilst the model simulates only ~ 0.2 pptV underestimating HONO at all times. It is clear that long-range transport and thermal decomposition of NO_y species such as PAN alone cannot explain the NO_x diurnal at Cape Verde. A PAN-type continuous thermal decomposition forming NO_x would be inconsistent with the diurnal maximum in NO_x which is observed. The NO_x source necessary to support a noon time maximum would have to show a strong day-time maximum to counter the strong diurnal in the sink.

This need for a diurnal cycle in the NO_x source also suggests that the shipping source of NO_x is unlikely to explain the diurnal cycle. The dominant source of ship NO_x in the region occurs from

the large container ships which pass the region on their way to South America or the Cape of Good Hope. It is unlikely that these emissions are systematically higher during the day than during the night and thus are unlikely to explain the observed diurnal signal.

There have been a number of studies which have identified much faster photolysis of nitrate within and on aerosol, than for gas phase nitric acid. These include studies using real-world natural and artificial surfaces (Baergen and Donaldson, 2013; Ye et al., 2016a, 2016b), laboratory substrates such as organic films and aqueous acid solutions (Handley et al., 2007; Scharko et al., 2014; Zhou et al., 2003), aerosol nitrate (Ndour et al., 2009; Ye et al., 2016b), and a model estimate (Cohan et al., 2008). These studies have found that particulate nitrate photolysis rates can be up to ~3 orders of magnitude greater than gas phase HNO_3 photolysis in marine boundary layer conditions (Ye et al., 2016b). There is also broad agreement between different studies on the main photolysis product being nitrous acid (HONO) with NO_2 as a secondary species. The product ratio appears dependent on aerosol pH, with HONO production only occurring at low pH (Scharko et al., 2014). This is shown in reaction (R6) as particulate nitrate (p-NO_3) photolysing to HONO and NO_2 in a ratio *x*:*y*.

$$\text{p-NO}_3 + h\nu \rightarrow x\text{HONO} + y\text{NO}_2 \qquad \text{(R6)}$$

There is also evidence that the photolysis rate is positively correlated with relative humidity (Baergen and Donaldson, 2013; Scharko et al., 2014). As such, particulate nitrate photolysis rates appear to increase with increasing aerosol acidity and relative humidity. With the CVO site experiencing relative humidity of 79 % on average (Carpenter et al., 2010) and aerosol containing a significant acidic fraction (Fomba et al., 2014), particulate nitrate photolysis could have a role to play in the NO_x budget at Cape Verde.

In order to explore the implications for Cape Verde NO_x chemistry, we re-ran the base model removing the PAN source but including particulate nitrate (p-NO_3) photolysis (R6) leading to HONO and NO_2 production, scaled to the gas phase photolysis of HNO_3. This parameterisation nominally represents photolysis of nitrate within and on aerosol, however conceptually includes any additional surface production of HONO and NO_2. We use an aerosol phase concentration of nitrate of 1.1 μg m^{-3} (equivalent to 400 pptV), which is the mean concentration found in PM10

aerosol at Cape Verde, with little apparent seasonal variability (Fomba et al., 2014; Savarino et al., 2013). The branching ratio of HONO to NO_2 production from reaction 6 (*x* and *y*) was set to 2:1 in line with the findings of Ye et al., (2016b). We scale the p-NO_3 photolysis rate to gas phase HNO_3 photolysis by factors of 1, 10, 25, 50, 100, and 1000. The study of Ye et al., (2016b) describes enhancements of up to ~300 fold. The impact on the summer months is shown in Fig. 4.

Including the photolysis of aerosol nitrate changes both the mean concentration and diurnal cycle of NO_x significantly. The diurnal NO_x is now flat or peaks during the daytime, more consistent with observations. We find the best approximation is achieved when the rate of particulate nitrate photolysis is ~10 times that of HNO_3 which is broadly consistent with laboratory based observations (Zhou et al., 2003). A wide variability of p-NO_3 photolysis rates on different surfaces are reported (Ye et al., 2016a), thus the photolysis of nitrate is uncertain and likely to be variable with aerosol composition. In all particulate nitrate photolysis-only scenarios, depicted in Fig. 4 and Fig. 5, it is evident that p-NO_3 photolysis alone doesn't give the observed increase in night time NO_x observations. Conversely the PAN only scenario is insufficient to sustain daytime NO_x. It is therefore likely that the actual source of NO_x is a combination of PAN entrainment from the free troposphere and particulate nitrate photolysis.

Combining the free-tropospheric source of PAN, and the photolysis of particulate nitrate at a rate of 10 times the gas phase HNO_3 photolysis (Fig. 5) results in a model simulation with roughly twice as much NO_x both at night and during daylight but a roughly flat diurnal profile. Simulated HONO peaks at local noon, similar to the observations though underestimates the mid-day peak. Nocturnal HONO mixing ratios agree with observations being non-zero at ~0.5 pptV.

Introduction of an additional source of NO_x is able to roughly produce a flat diurnal cycle, though is not able to simulate a definite peak of NO_x during daytime. With the addition of a source and no change in sinks for NO_x this is unsurprising and leads to relative over estimation of NO_x particularly at night. This is therefore likely that one or more NO_x sinks are absent from the base simulation which must be explored further.

3.3 NO_x sinks

Aside from loss to HNO_3 directly through reaction with OH (R1) NO_x is also lost to nitrate by reaction with halogen oxides (XO) forming a halogen nitrates (R7) (Keene et al., 2009). Read et al., (2008) showed how halogen oxides mediate ozone formation and loss at Cape Verde thus also exerting an indirect effect on NO_x.

$$XO + NO_2 + M \rightarrow XONO_2 + M \qquad \text{(R7)}$$

Figure 6 shows the rates of production and loss analysis for NO_x in this simulation with both PAN thermal decomposition and particulate nitrate photolysis. The largest net source of NO_x after net sinks (such as halogen nitrate cycling) are removed is nitrate photolysis to HONO and NO_2. The major net sink of NO_x is the formation of nitric acid by reaction of NO_2 with OH. – However, uptake of HNO_3 onto aerosol, and subsequent rapid (compared to gas phase HNO_3) photolysis acts to balance this.

The pronounced drop in modelled NO_2 at sunrise is due to production of halogen nitrates (R7) when HOX rapidly photolyses to produce XO which can then react with NO_2 to produce $XONO_2$. XO is formed quickly and spikes in concentration leading to the rapid loss of NO_2. This feature is not observed in the NO_x observations during any season.

The diagnostics in Figure 6 show the role of the different sinks of NO_x. In that simulation these are dominated by the gas phase reaction between NO_2 and OH but with the rapid formation and subsequent hydrolysis of $BrONO_2$ and $IONO_2$ (R8) playing a major role (Sander et al., 1999). The uptake coefficient (γ) of halogen nitrates onto aerosol therefore could have a strong influence on the NO_x diurnal.

$$XONO_2 + H_2O_{(aer)} \rightarrow HNO_{3(aer)} + X^+ + OH^- \qquad \text{(R8)}$$

We perform a sensitivity analysis on the effect of the uptake coefficients on the NO_x and XO diurnals. We do this in a particulate nitrate photolysis only simulation, without PAN, to isolate the effect of $XONO_2$ hydrolysis on nitrate-NO_x cycling. Figure 7 shows the effect of changing γ of $XONO_2$ (X = Br, I) within recommended ranges (Burkholder et al., 2015; Saiz-Lopez et al., 2008) on Saharan dust and sea salt – the predominant coarse mode aerosol by mass at Cape Verde (Carpenter et al., 2010; Fomba et al., 2014), ranging from 0.02 to 0.8.

Increasing the γ of $XONO_2$ from 0.02 (the low end of recommended values) to 0.1 results in small changes to both the NO_x and XO diurnals. The loss of NO_x at sunrise becomes more pronounced whereas the XO diurnals become slightly more 'square' or 'top-hat' as per the observations of Read et al., (2008). Increasing the γ to the upper extreme (γ = 0.8) results in a spike in BrO at sunrise, which consumes the majority of NO_2 though formation of $BrONO_2$. No combination of uptake coefficients can completely reproduce the characteristic XO diurnals due to poor constraints on heterogeneous halogen chemistry (Abbatt et al., 2012) in addition to gaps in understanding of gas phase halogen chemistry (Simpson et al., 2015).

The effect on the NO_x diurnal of changing γ is clear in that greater uptake coefficients recommended by Burkholder et al., (2015) result in objectively worse simulation of both the NO_x and XO diurnals. It is therefore likely that information is lacking from the XO – NO_x chemistry scheme as it is currently known.

3.4 HOI/HOBr - NO_x chemistry

Recently, IO recycling by reaction with NO_3 has been proposed by Saiz-Lopez et al., (2016) who calculated that the reaction (R9) of HOI + NO_3 producing IO and HNO_3 has a low enough activation energy and fast enough rate constant to be atmospherically relevant in the troposphere.

$$HOI + NO_3 \rightarrow IO + HNO_3 \quad : \quad k = 2.7 \times 10^{-12} (300/T)^{2.66} \qquad \text{(R9)}$$

This mechanism provides a route to nitric acid, and thus particulate nitrate at night, whilst also leading to nocturnal IO production leading to loss of NO_2 by $IONO_2$ formation.

Including this new reaction and re-running the model leads to a diurnal profile of IO much more representative of the observations. This however introduces a more pronounced loss of NO_x at sunrise and sunset, and also results in NO_x peaking during the day which fits better with the observations as shown in Fig. 8. HONO is still underestimated during daytime though nocturnal values agree well.

The inclusion of this HOI + NO_3 reaction reproduces the general NO_x and O_3 diurnals more closely than without i.e. a daytime maximum in NO_x. There are also effects on the halogen oxide

behaviour. The simulated BrO has a flatter profile, which more closely matches the observations. However, modelled IO is now non-zero at night and the sunrise build-up and sunset decay still occurs more abruptly than the observations.

Although the NO_x and O_3 diurnals are reproduced more closely with this new chemistry, there is still disagreement with the observed NO_x diurnal at sunrise and sunset especially indicating a missing reaction or reactions. To best approximate the observed diurnal behaviour an analogous HOBr + NO_3 night time reaction (R10) was introduced with a rate 10 times that of HOI + NO_3 as calculated by Saiz-Lopez et al., (2016b)

$$HOBr + NO_3 \rightarrow BrO + HNO_3 \quad : \quad k = 2.7 \times 10^{-11} (300/T)^{2.66} \qquad (R10)$$

This results in an improved reproduction of the observed NO_x diurnal, Fig. 9. This is a purely speculative representation in order to reproduce the observed NO_x diurnal and highlights how some mechanistic knowledge of NO_x-halogen-aerosol systems is still missing.

With HOX + NO_3 chemistry included in the model as in Fig. 9, significant loss of NO_x at sunrise and sunset is eliminated and agreement is improved over any previous simulation. Greater HONO production is also simulated, with up to ~ 3.0.pptV predicted – in line with the observations shown in Fig. 2. Halogen oxide modelled diurnal cycles remain broadly consistent with observations. Diagnosis of the net production and loss terms for NO_x reveal that nitrate photolysis to HONO or NO_2 contribute ~ 80% of all NO_x with decomposition of PAN contributing the remainder. Major net sinks of NO_x are shown to be reaction with halogen hydroxides and OH to form HNO_3. Nitric acid is then taken up on surfaces and recycled to NO_x through photolysis to NO_2 and HONO

The improvement can be better understood by diagnosing the modelled NO_y distribution. In Fig. 10 the distribution of PAN, $IONO_2$, $BrONO_2$, N_2O_5, NO_3 and particulate nitrate (p-NO_3) is shown for the base case scenario (where entrained PAN is the sole source of NO_x in the MBL), for the particulate nitrate photolysis case including HOI + NO_3 chemistry, and the same but also including HOBr + NO_3 chemistry. The major feature changing through the different simulations is the magnitude and shape of the $BrONO_2$ diurnal. From the base run to the inclusion of HOI +

NO_3 chemistry and particulate nitrate photolysis a major increase in $BrONO_2$ mixing ratio is expected at sun rise and sun set. It is this rapid production of $BrONO_2$ which consumes NO_x resulting in the sharp dips at these times not seen in the observations. In the HOBr & HOI + NO_3 and particulate nitrate photolysis case these features are eliminated and halogen nitrates do not spike at sunrise or sunset. Nitrate is shown to be conserved by hydrolysis of halogen nitrates on surfaces and uptake of nitric acid. This cycling leads to a NO_x diurnal profile which is more representative of the observations.

In models which included nitrate photolysis a strong diurnal cycle in particulate nitrate presents which is depleted during the day and recycles at night being conserved overall. The daily average concentration remains constant however in line with integrating filter sample study of Fomba et al., (2014).

Unsurprisingly, the inclusion of HOX + NO_3 chemistry results in lower mixing ratios of NO_3 at night. In all cases N_2O_5 (in black) is effectively zero at all times due to very low NO_x mixing ratios in this pristine environment and the relatively high ambient temperatures (24.5 ^oC) where the N_2O_5 lifetime is ~ 3 s^{-1}. This precludes N_2O_5 channels to NO_x (and ultimately nitrate), consistent with the experimental findings of Savarino et al., (2013) at Cape Verde who found isotope ratios which were incompatible with high production rates of HNO_3 from N_2O_5 hydrolysis, and concluded that N_2O_5 and nitryl compound ($ClNO_2$, $BrNO_2$) levels in this region are very low. This is consistent with our own and other studies modelling the pristine marine boundary layer at Cape Verde of Sommariva and Von Glasow, (2012). This is in contrast with more polluted regions where N_2O_5 has been shown to be a route to NO_x and $ClNO_2$ (Kim et al., 2014).

The agreement in modelled and observed NO_x improves and the modelled values fall within the error of the observations. Additionally the approximate BrO diurnal is achieved – without the characteristic 'horns', however replicating IO observations is still problematic.

The effect of dramatically changing NO_x diurnal could be expected to have an effect on OH and HO_2 mixing ratios. The difference between the base model case, where PAN decomposition is

the dominant daytime source, and the final model where the NO_x is more accurately described by particulate nitrate photolysis and HOX + NO_3 chemistry is shown in Fig. 11.

In the case of OH the change from the base model to the final model is an increase of 3.3% at the maximum, for HO_2 the increase is a more significant 8.6% (or 1.7 pptV), however this is well within the uncertainty of measured values (Whalley et al., 2010). Figure 11 shows that even with dramatic changes in the NO_x simulation, the OH and HO_2 changes very little comparatively despite increased daytime HONO production.

From these simulations it would appear that the photolysis of surface adsorbed nitrate may be the dominant source of NO_x into the marine boundary layer around Cape Verde. Photolysis of aerosol nitrate, or nitrate in solution would be capable of producing a diurnal cycle in NO_x which was consistent with the observations when HOX + NO_3 chemistry is considered also. Whilst agreement between model and observation is improved there is a clear gap in understanding the halogen-NO_x-aerosol system in the remote marine boundary layer.

4 Conclusions

Fast aerosol nitrate photolysis is shown to be likely the primary source of NO_x in the remote tropical Atlantic boundary layer. A 0-D model replicated the observed halogen, O_3, OH, NO_x and HONO levels when including particulate nitrate photolysis at a rate of ~10 times that of gas phase nitric acid, consistent with previous laboratory measurements. Model optimisation shows that this new source of daytime NO_2 is compatible with observations and currently known chemistry at night and at mid-day, but that at sunrise and sunset there is disagreement due to the treatment of halogen oxides at these times. Recently suggested halogen hydroxide + nitrate radical chemistry may provide better agreement between model and observation if theoretical reactions can be substantiated.

Data Availability

We thank the NASA Jet Propulsion Laboratory (Burkholder et al., 2015) for providing comprehensive rate and uptake coefficient data for atmospheric compounds, which can be found at http://jpldataeval.jpl.nasa.gov.

All data used in this work is available from the British Atmospheric Data Centre (BADC) http://badc.nerc.ac.uk and is included as a .csv file in the supplementary information. The DSMACC model is available from https://github.com/barronh/DSMACC and a full description of the model can be found in the supplementary information.

Acknowledgements. The authors would like to thank Luis Neves Mendes of the Instituto Nacional de Meteorologia e Geofísica (INMG) for their operational support at the CVO site. The financial support of the National Centre for Atmospheric Science (NCAS) for supporting the CVO measurement program, and of the Natural Environmental Research Council (NERC) for supporting the studentship of Chris Reed is gratefully acknowledged. HONO measurements were support by NERC grant NE/M013545/1 (Sources of Nitrous Acid in the Atmospheric Boundary Layer).

References

Abbatt, J. P. D., Lee, A. K. Y. and Thornton, J. A.: Quantifying trace gas uptake to tropospheric aerosol: recent advances and remaining challenges, Chem. Soc. Rev., 41(19), 6555, doi:10.1039/c2cs35052a, 2012.

Baergen, A. M. and Donaldson, D. J.: Photochemical renoxification of nitric acid on real urban grime, Environ. Sci. Technol., 47(2), 815–820, doi:10.1021/es3037862, 2013.

Baergen, A. M. and Donaldson, D. J.: Formation of reactive nitrogen oxides from urban grime photochemistry, Atmos. Chem. Phys., 16(10), 6355–6363, doi:10.5194/acp-16-6355-2016, 2016.

Beirle, S., Platt, U., von Glasow, R., Wenig, M. and Wagner, T.: Estimate of nitrogen oxide emissions from shipping by satellite remote sensing, Geophys. Res. Lett., 31(18), 4–7, doi:10.1029/2004GL020312, 2004.

Burkholder, J. B., Sander, S. P., Abbatt, J., Barker, J. R., Huie, R. E., Kolb, C. E., Kurylo, M. J., Orkin, V. L., Wilmouth, D. M. and Wine, P. H.: Chemical Kinetics and Photochemical Data for Use in Atmospheric Studies, Evaluation No. 18, JPL Publ. 15-10, 15(10), 2015.

Carpenter, L. J., Fleming, Z. L., Read, K. A., Lee, J. D., Moller, S. J., Hopkins, J. R., Purvis, R. M., Lewis, A. C., Müller, K., Heinold, B., Herrmann, H., Fomba, K. W., Pinxteren, D., Müller, C., Tegen, I., Wiedensohler, A., Müller, T., Niedermeier, N., Achterberg, E. P., Patey, M. D., Kozlova, E. A., Heimann, M., Heard, D. E., Plane, J. M. C., Mahajan, A., Oetjen, H., Ingham, T., Stone, D., Whalley, L. K., Evans, M. J., Pilling, M. J., Leigh, R. J., Monks, P. S., Karunaharan, A., Vaughan, S., Arnold, S. R., Tschritter, J., Pöhler, D., Frieß, U., Holla, R., Mendes, L. M., Lopez, H., Faria, B., Manning, A. J. and Wallace, D. W. R.: Seasonal characteristics of tropical marine boundary layer air measured at the Cape Verde Atmospheric Observatory, J. Atmos. Chem., 67(2–3), 87–140, doi:10.1007/s10874-011-9206-1, 2010.

Carsey, T. P., Churchill, D. D., Farmer, M. L., Fischer, C. J., Pszenny, A. A., Ross, V. B., Saltzman, E. S., Springer-Young, M., Bonsang, B., Boss, V. B., Saltzmann, E. S., Springer-Young, M. and Bonsang, B.: Nitrogen oxides and ozone production in the North Atlantic marine boundary layer, J. Geophys. Res. Atmos., 102(D9), 653–665, doi:10.1029/96JD03511, 1997.

Clough, P. N. and Thrush, B. A.: Mechanism of chemiluminescent reaction between nitric oxide and ozone, Trans. Faraday Soc., 63(2), 915, doi:10.1039/tf9676300915, 1967.

Cohan, A., Chang, W., Carreras-Sospedra, M. and Dabdub, D.: Influence of sea-salt activated chlorine and surface-mediated renoxification on the weekend effect in the South Coast Air Basin of California, Atmos. Environ., 42(13), 3115–3129, doi:10.1016/j.atmosenv.2007.11.046, 2008.

Dickerson, R. R., Rhoads, K. P., Carsey, T. P., Oltmans, S. J., Burrows, J. P. and Crutzen, P. J.: Ozone in the remote marine boundary layer: A possible role for halogens, J. Geophys. Res., 104(D17), 21,385-21,395, doi:10.1029/1999JD900023, 1999.

Drummond, J. W., Volz, A. and Ehhalt, D. H.: An optimized chemiluminescence detector for tropospheric NO measurements, J. Atmos. Chem., 2(3), 287–306, doi:10.1007/BF00051078, 1985.

Emmerson, K. M. and Evans, M. J.: Comparison of tropospheric gas-phase chemistry schemes for use within global models, Atmos. Chem. Phys., (1990), 1831–1845, doi:10.5194/acpd-8-19957-2008, 2009.

Evans, M. J.: Impact of new laboratory studies of N_2O_5 hydrolysis on global model budgets of tropospheric nitrogen oxides, ozone, and OH, Geophys. Res. Lett., 32(9), L09813, doi:10.1029/2005GL022469, 2005.

Fischer, E. V., Jacob, D. J., Yantosca, R. M., Sulprizio, M. P., Millet, D. B., Mao, J., Paulot, F., Singh, H. B., Roiger, A.-E., Ries, L., Talbot, R. W., Dzepina, K. and Pandey Deolal, S.: Atmospheric peroxyacetyl nitrate (PAN): a global budget and source attribution, Atmos. Chem. Phys., 14(5), 2679–2698, doi:10.5194/acp-14-2679-2014, 2014.

Fomba, K. W., Müller, K., Van Pinxteren, D., Poulain, L., Van Pinxteren, M. and Herrmann, H.: Long-term chemical characterization of tropical and marine aerosols at the Cape Verde Atmospheric Observatory (CVAO) from 2007 to 2011, Atmos. Chem. Phys., 14(17), 8883–8904,

doi:10.5194/acp-14-8883-2014, 2014.

Handley, S. R., Clifford, D. and Donaldson, D. J.: Photochemical Loss of Nitric Acid on Organic Films: a Possible Recycling Mechanism for NO_x, Environ. Sci. Technol., 41(11), 3898–3903, doi:10.1021/es062044z, 2007.

Heland, J., Kleffmann, J., Kurtenbach, R. and Wiesen, P.: A new instrument to measure gaseous nitrous acid (HONO) in the atmosphere, Environ. Sci. Technol., 35(15), 3207–3212, doi:10.1021/es000303t, 2001.

Jacobi, H.-W.-W., Weller, R., Bluszcz, T. and Schrems, O.: Latitudinal distribution of peroxyacetyl nitrate (PAN) over the Atlantic Ocean, J. Geophys. Res., 104(D21), 26901–26912, doi:10.1029/1999JD900462, 1999.

Keene, W. C., Long, M. S., Pszenny, A. A. P., Sander, R., Maben, J. R., Wall, A. J., O'Halloran, T. L., Kerkweg, A., Fischer, E. V., and Schrems, O.: Latitudinal variation in the multiphase chemical processing of inorganic halogens and related species over the eastern North and South Atlantic Oceans, Atmos. Chem. Phys., 9, 7361-7385, doi:10.5194/acp-9-7361-2009, 2009.

Keene, W. C., Stutz, J., Pszenny, A. A. P., Maben, J. R., Fischer, E. V., Smith, A. M., von Glasow, R., Pechtl, S., Sive, B. C. and Varner, R. K.: Inorganic chlorine and bromine in coastal New England air during summer, J. Geophys. Res., 112(D10), D10S12, doi:10.1029/2006JD007689, 2007.

Kim, M. J., Farmer, D. K. and Bertram, T. H.: A controlling role for the air-sea interface in the chemical processing of reactive nitrogen in the coastal marine boundary layer, Proc. Natl. Acad. Sci., 111(11), 1–6, doi:10.1073/pnas.1318694111, 2014.

Kleffmann, J. and Wiesen, P.: Technical note: Quantification of interferences of wet chemical HONO LOPAP measurements under simulated polar conditions, Atmos. Chem. Phys., 8(22), 6813–6822, doi:10.5194/acp-8-6813-2008, 2008.

Lawler, M. J., Finley, B. D., Keene, W. C., Pszenny, A. A. P., Read, K. A., Von Glasow, R. and Saltzman, E. S.: Pollution-enhanced reactive chlorine chemistry in the eastern tropical Atlantic boundary layer, Geophys. Res. Lett., 36(8), 3–7, doi:10.1029/2008GL036666, 2009.

Lee, J. D., Moller, S. J., Read, K. A., Lewis, A. C., Mendes, L. and Carpenter, L. J.: Year-round measurements of nitrogen oxides and ozone in the tropical North Atlantic marine boundary layer, J. Geophys. Res., 114(D21), D21302, doi:10.1029/2009JD011878, 2009.

Lewis, A. C., Evans, M. J., Methven, J., Watson, N., Lee, J. D., Hopkins, J. R., Purvis, R. M., Arnold, S. R., McQuaid, J. B., Whalley, L. K., Pilling, M. J., Heard, D. E., Monks, P. S., Parker, A. E., Reeves, C. E., Oram, D. E., Mills, G., Bandy, B. J., Stewart, D., Coe, H., Williams, P. and Crosier, J.: Chemical composition observed over the mid-Atlantic and the detection of pollution signatures far from source regions, J. Geophys. Res., 112(D10), D10S39, doi:10.1029/2006JD007584, 2007.

Li, X., Rohrer, F., Hofzumahaus, A., Brauers, T., Haseler, R., Bohn, B., Broch, S., Fuchs, H., Gomm, S., Holland, F., Jager, J., Kaiser, J., Keutsch, F. N., Lohse, I., Lu, K., Tillmann, R., Wegener, R., Wolfe, G. M., Mentel, T. F., Kiendler-Scharr, A. and Wahner, A.: Missing Gas-Phase Source of HONO Inferred from Zeppelin Measurements in the Troposphere, Science (80-.)., 344(6181), 292–296, doi:10.1126/science.1248999, 2014.

Mahajan, A. S., Plane, J. M. C., Oetjen, H., Mendes, L., Saunders, R. W., Saiz-Lopez, A., Jones, C. E., Carpenter, L. J. and McFiggans, G. B.: Measurement and modelling of tropospheric reactive halogen species over the tropical Atlantic Ocean, Atmos. Chem. Phys., 10(10), 4611–4624, doi:10.5194/acp-10-4611-2010, 2010.

Monks, P. S., Carpenter, L. J., Penkett, S. A., Ayers, G. P., Gillett, R. W., Galbally, I. E. and Meyer, C. P.: Fundamental ozone photochemistry in the remote marine boundary layer: The SOAPEX experiment, measurement and theory, Atmos. Environ., 32(21), 3647–3664, doi:10.1016/S1352-2310(98)00084-3, 1998.

Moxim, W. J., Levy, H. and Kasibhatla, P. S.: Simulated global tropospheric PAN: Its transport and impact on NO_x, J. Geophys. Res. Atmos., 101(D7), 12621–12638, doi:10.1029/96JD00338, 1996.

Nakamura, K., Kondo, Y., Chen, G., Crawford, J. H., Takegawa, N., Koike, M., Kita, K., Miyazaki, Y., Shetter, R. E., Lefer, B. L., Avery, M. and Matsumoto, J.: Measurement of NO_2 by the photolysis conversion technique during the Transport and Chemical Evolution Over the Pacific (TRACE-P) campaign, J. Geophys. Res. Atmos., 108(D24), ACH 1-ACH 11, doi:10.1029/2003JD003712, 2003.

Ndour, M., Conchon, P., D'Anna, B., Ka, O. and George, C.: Photochemistry of mineral dust surface as a potential atmospheric renoxification process, Geophys. Res. Lett., 36(5), L05816, doi:10.1029/2008GL036662, 2009.

Neu, J. L., Lawler, M. J., Prather, M. J. and Saltzman, E. S.: Oceanic alkyl nitrates as a natural source of tropospheric ozone, Geophys. Res. Lett., 35(13), L13814, doi:10.1029/2008GL034189, 2008.

Pollack, I. B., Lerner, B. M. and Ryerson, T. B.: Evaluation of ultraviolet light-emitting diodes for detection of atmospheric NO_2 by photolysis - chemiluminescence, J. Atmos. Chem., 65(2–3), 111–125, doi:10.1007/s10874-011-9184-3, 2011.

Pszenny, A. A. P., Moldanová, J., Keene, W. C., Sander, R., Maben, J. R., Martinez, M., Crutzen, P. J., Perner, D. and Prinn, R. G.: Halogen cycling and aerosol pH in the Hawaiian marine boundary layer, Atmos. Chem. Phys., 4(1), 147–168, doi:10.5194/acp-4-147-2004, 2004.

Read, K. A., Carpenter, L. J., Arnold, S. R., Beale, R., Nightingale, P. D., Hopkins, J. R., Lewis, A. C., Lee, J. D., Mendes, L. and Pickering, S. J.: Multiannual observations of acetone, methanol, and acetaldehyde in remote tropical atlantic air: implications for atmospheric OVOC budgets and oxidative capacity., Environ. Sci. Technol., 46(20), 11028–39,

doi:10.1021/es302082p, 2012.

Read, K. A., Mahajan, A. S., Carpenter, L. J., Evans, M. J., Faria, B. V. E., Heard, D. E., Hopkins, J. R., Lee, J. D., Moller, S. J., Lewis, A. C., Mendes, L., McQuaid, J. B., Oetjen, H., Saiz-Lopez, A., Pilling, M. J. and Plane, J. M. C.: Extensive halogen-mediated ozone destruction over the tropical Atlantic Ocean, Nature, 453(7199), 1232–1235, doi:10.1038/nature07035, 2008.

Reed, C., Brumby, C. A., Crilley, L. R., Kramer, L. J., Bloss, W. J., Seakins, P. W., Lee, J. D. and Carpenter, L. J.: HONO measurement by differential photolysis, Atmos. Meas. Tech., 9(6), 2483–2495, doi:10.5194/amt-9-2483-2016, 2016a.

Reed, C., Evans, M. J., Di Carlo, P., Lee, J. D. and Carpenter, L. J.: Interferences in photolytic NO_2 measurements: explanation for an apparent missing oxidant?, Atmos. Chem. Phys., 16(7), 4707–4724, doi:10.5194/acp-16-4707-2016, 2016b.

Ren, X., Gao, H., Zhou, X., Crounse, J. D., Wennberg, P. O., Browne, E. C., LaFranchi, B. W., Cohen, R. C., McKay, M., Goldstein, A. H. and Mao, J.: Measurement of atmospheric nitrous acid at Blodgett Forest during BEARPEX2007, Atmos. Chem. Phys., 10(13), 6501, doi:10.5194/acp-10-6283-2010, 2010.

Ridley, D. A., Heald, C. L. and Prospero, J. M.: What controls the recent changes in African mineral dust aerosol across the Atlantic?, Atmos. Chem. Phys., 14(11), 5735–5747, doi:10.5194/acp-14-5735-2014, 2014.

Ryerson, T. B., Williams, E. J. and Fehsenfeld, F. C.: An efficient photolysis system for fast-response NO_2 measurements, J. Geophys. Res., 105(2), 26,447-26,461, doi:10.1029/2000JD900389, 2000.

Saiz-Lopez, A., Plane, J. M. C., Cuevas, C. A., Mahajan, A. S., Lamarque, J.-F. and Kinnison, D. E.: Nighttime atmospheric chemistry of iodine, Atmos. Chem. Phys., 16(24), 15593–15604, doi:10.5194/acp-16-15593-2016, 2016.

Saiz-Lopez, A., Plane, J. M. C., Mahajan, A. S., Anderson, P. S., Bauguitte, S. J.-B., Jones, A. E., Roscoe, H. K., Salmon, R. A., Bloss, W. J., Lee, J. D. and Heard, D. E.: On the vertical distribution of boundary layer halogens over coastal Antarctica: implications for O_3, HO_x, NO_x and the Hg lifetime, Atmos. Chem. Phys., 8(4), 887–900, doi:10.5194/acp-8-887-2008, 2008.

Sander, R., Rudich, Y., von Glasow, R. and Crutzen, P. J.: The role of $BrNO_3$ in marine tropospheric chemistry: A model study, Geophys. Res. Lett., 26(18), 2857–2860, doi:10.1029/1999GL900478, 1999.

Savarino, J., Morin, S., Erbland, J., Grannec, F., Patey, M. D., Vicars, W., Alexander, B. and Achterberg, E. P.: Isotopic composition of atmospheric nitrate in a tropical marine boundary layer, Proc. Natl. Acad. Sci., 110(44), 17668–17673, doi:10.1073/pnas.1216639110, 2013.

Scharko, N. K., Berke, A. E. and Raff, J. D.: Release of Nitrous Acid and Nitrogen Dioxide from Nitrate Photolysis in Acidic Aqueous Solutions, Environ. Sci. Technol., 48(20), 11991–12001, doi:10.1021/es503088x, 2014.

Sherwen, T., Evans, M. J., Carpenter, L. J., Andrews, S. J., Lidster, R. T., Dix, B., Koenig, T. K., Sinreich, R., Ortega, I., Volkamer, R., Saiz-Lopez, A., Prados-Roman, C., Mahajan, A. S. and Ordóñez, C.: Iodine's impact on tropospheric oxidants: A global model study in GEOS-Chem, Atmos. Chem. Phys., 16(2), 1161–1186, doi:10.5194/acp-16-1161-2016, 2016.

Simpson, W. R., Brown, S. S., Saiz-Lopez, A., Thornton, J. A. and Von Glasow, R.: Tropospheric Halogen Chemistry: Sources, Cycling, and Impacts, Chem. Rev., 115(10), 4035–4062, doi:10.1021/cr5006638, 2015.

Sommariva, R. and Von Glasow, R.: Multiphase halogen chemistry in the tropical atlantic ocean, Environ. Sci. Technol., 46(19), 10429–10437, doi:10.1021/es300209f, 2012.

VandenBoer, T. C., Markovic, M. Z., Sanders, J. E., Ren, X., Pusede, S. E., Browne, E. C., Cohen, R. C., Zhang, L., Thomas, J., Brune, W. H. and Murphy, J. G.: Evidence for a nitrous acid (HONO) reservoir at the ground surface in Bakersfield, CA, during CalNex 2010, J. Geophys. Res. Atmos., 119(14), 9093–9106, doi:10.1002/2013JD020971, 2014.

Vogt, R., Sander, R., Von Glasow, R. and Crutzen, P. J.: Iodine chemistry and its role in halogen activation and ozone loss in the marine boundary layer: A model study, J. Atmos. Chem., 32, 375–395, doi:10.1023/A:1006179901037, 1999.

Whalley, L. K., Furneaux, K. L., Goddard, A., Lee, J. D., Mahajan, A., Oetjen, H., Read, K. A., Kaaden, N., Carpenter, L. J., Lewis, A. C., Plane, J. M. C., Saltzman, E. S., Wiedensohler, A. and Heard, D. E.: The chemistry of OH and HO_2 radicals in the boundary layer over the tropical Atlantic Ocean, Atmos. Chem. Phys., 10(4), 1555–1576, doi:10.5194/acp-10-1555-2010, 2010.

Wojtal, P., Halla, J. D. and McLaren, R.: Pseudo steady states of HONO measured in the nocturnal marine boundary layer: A conceptual model for HONO formation on aqueous surfaces, Atmos. Chem. Phys., 11(7), 3243–3261, doi:10.5194/acp-11-3243-2011, 2011.

Ye, C., Gao, H., Zhang, N. and Zhou, X.: Photolysis of Nitric Acid and Nitrate on Natural and Artificial Surfaces, Environ. Sci. Technol., acs.est.5b05032, doi:10.1021/acs.est.5b05032, 2016a.

Ye, C., Zhou, X., Pu, D., Stutz, J., Festa, J., Spolaor, M., Tsai, C., Cantrell, C., Mauldin, R. L., Campos, T., Weinheimer, A., Hornbrook, R. S., Apel, E. C., Guenther, A., Kaser, L., Yuan, B., Karl, T., Haggerty, J., Hall, S., Ullmann, K., Smith, J. N., Ortega, J. and Knote, C.: Rapid cycling of reactive nitrogen in the marine boundary layer, Nature, 532(7600), 489–491, doi:10.1038/nature17195, 2016b.

Zhou, X., Civerolo, K., Dai, H., Huang, G., Schwab, J. and Demerjian, K.: Summertime nitrous acid chemistry in the atmospheric boundary layer at a rural site in New York State, J. Geophys. Res. Atmos., 107(D21), ACH 13-1-ACH 13-11, doi:10.1029/2001JD001539, 2002.

Zhou, X., Gao, H., He, Y., Huang, G., Bertman, S., Civerolo, K. and Schwab, J.: Nitric acid photolysis on surfaces in low-NO_x environments: significant atmospheric implications, Geophys. Res. Lett., 30(23), ASC 12/1--ASC 12/4, doi:10.1029/2003GL018620, 2003.

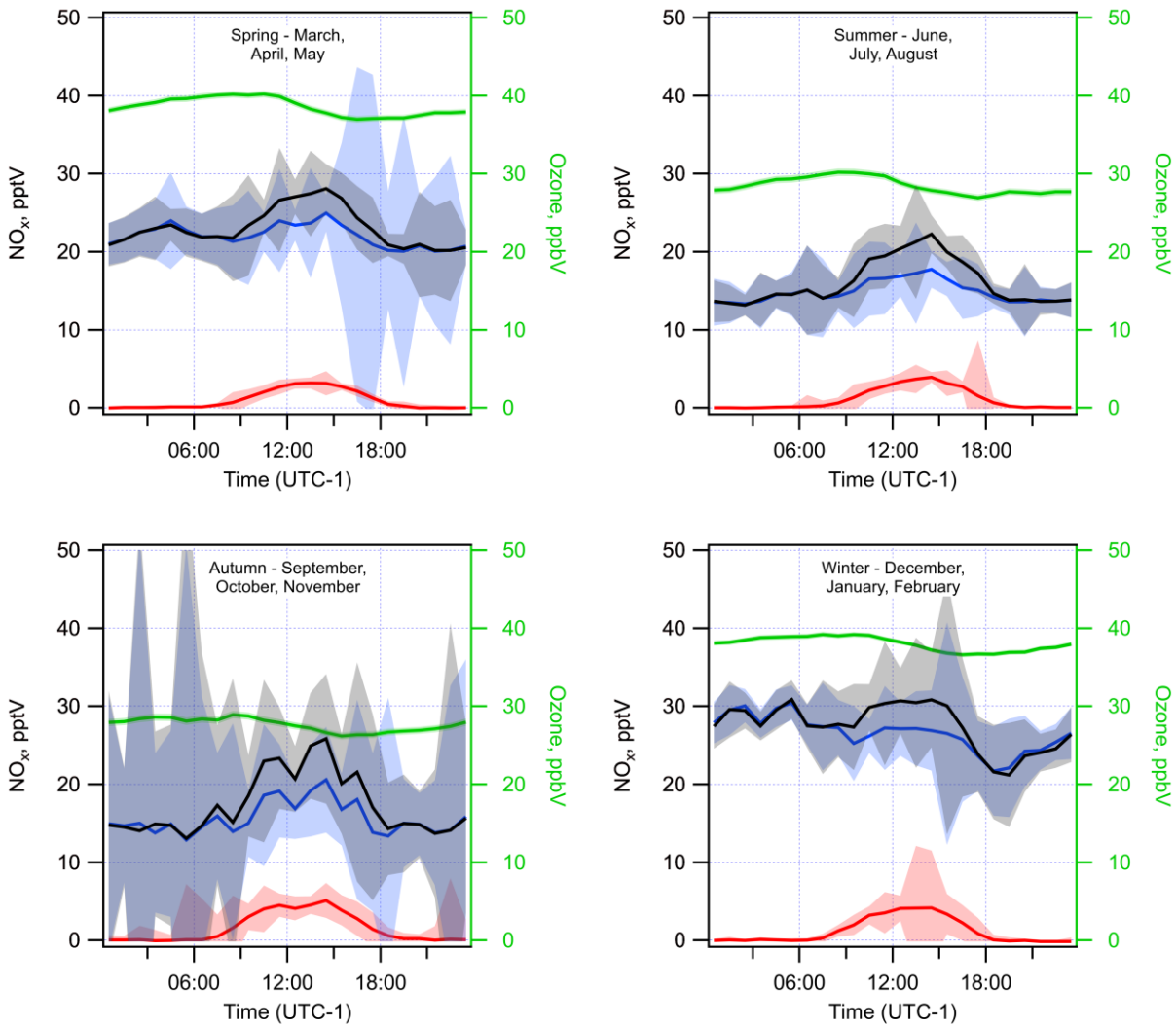

Figure 1. The observed seasonal diurnal cycles in NO, NO_2, NO_x, and O_3 at the CVO GAW station during 2014 and 2015. NO is shown in red, NO_2 in blue, NO_x in black, and O_3 in green. Shaded areas indicate the standard error of data.

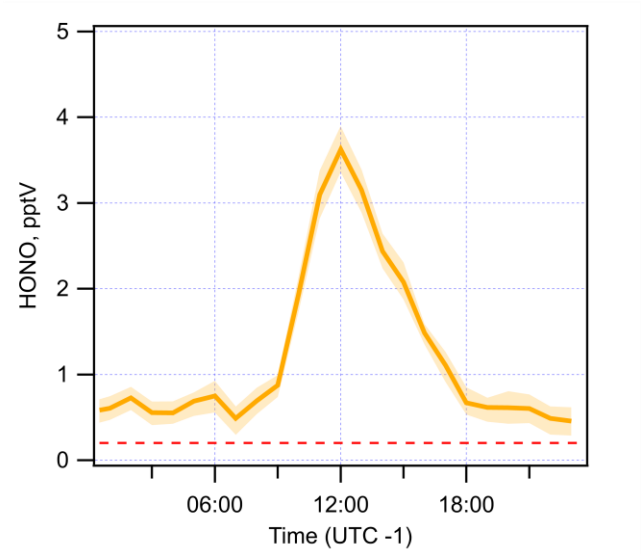

Figure 2. The observed average HONO diurnal measured at CVO during 24th November – 3rd December 2015. Shaded area indicates standard deviation and cumulative error of data. Dashed red line shows the HONO limit of detection.

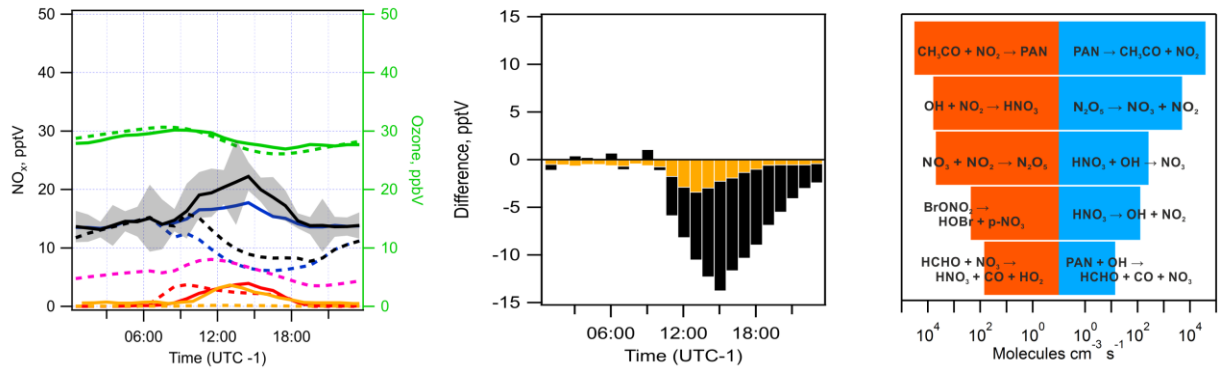

Figure 3. Left shows the measured (solid lines) and modelled (dashed) NO_x and HONO diurnal behaviour at the CVO GAW station where the dominant source of NO_x is a source of PAN descending from the upper troposphere having been transported from polluted regions. Shaded areas are standard error of the observations (NO_x N = 153 HONO, N = 10).O_3 – green; NO_x – black; NO_2 – blue; NO – red; HONO – yellow; PAN – pink. Centre is the difference between measured and modelled NO_x (black) and HONO (Yellow).Right shows the rates of production and loss of NO and NO_2 from sources listed in descending order of contribution over a 24 hour period accounting for >95% of the total.

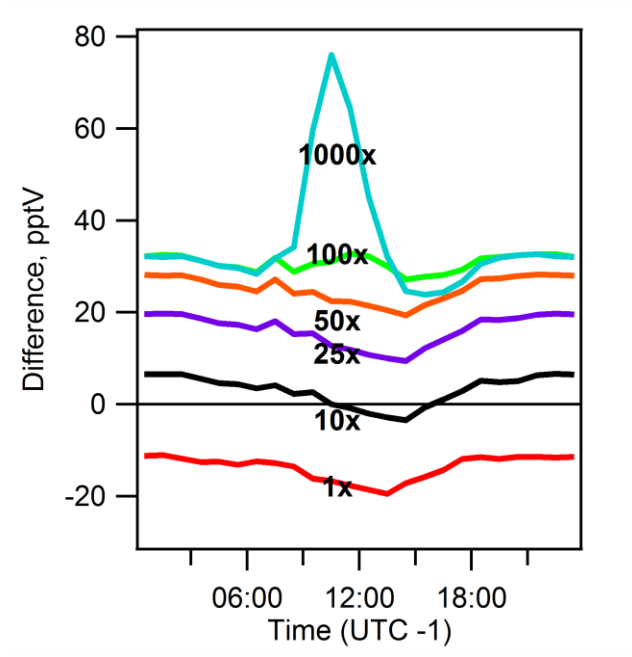

Figure 4. The difference between measured and modelled of NO_x at CVO during summer months when photolysis of nitrate is considered. The rate of particulate nitrate photolysis has been scaled to the rate of HNO_3 photolysis by factors of 1, 10, 25, 50, 100, and 1000.

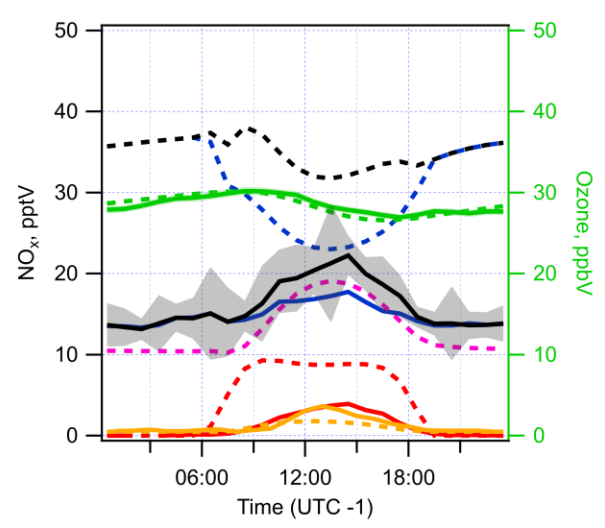

Figure 5. The modelled diurnal profile of NO_x at CVO during summer months when photolysis of nitrate (set at 10× the gas phase HNO_3 photolysis) and a tropospheric PAN source are considered. Shaded areas for NO_x are the standard error of the observation. O_3 – green; NO_x – black; NO_2 – blue; NO – red; HONO – yellow; PAN – pink.

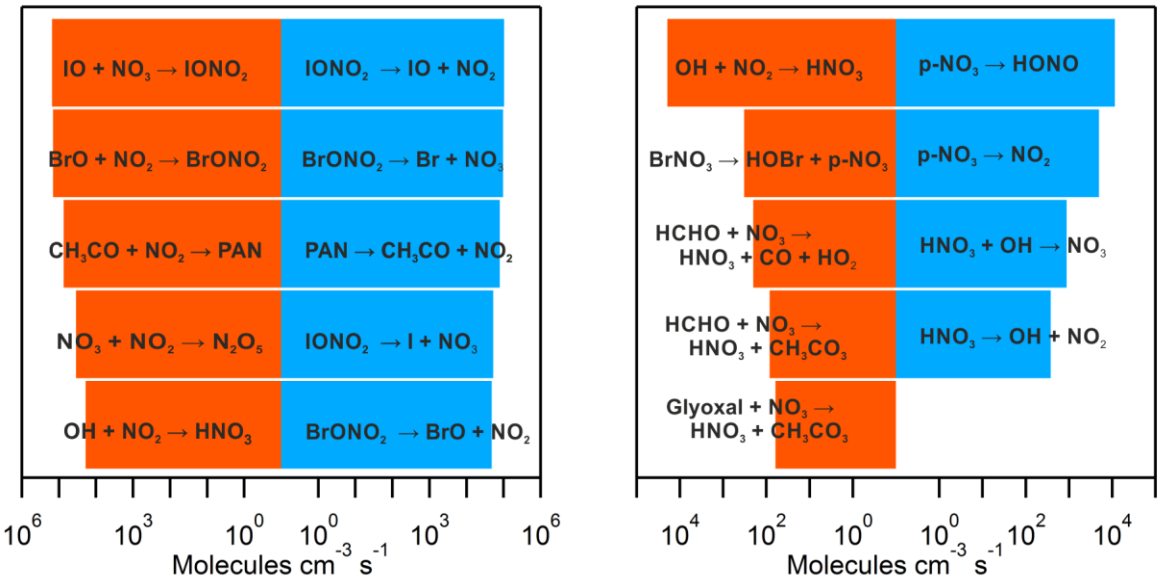

Figure 6. Left is the total production and loss analysis for NO_x of the combined model of particulate nitrate photolysis and PAN decomposition over 24 hours. Right is the same analysis discarding the major balanced sinks of fast cycling short lived species.

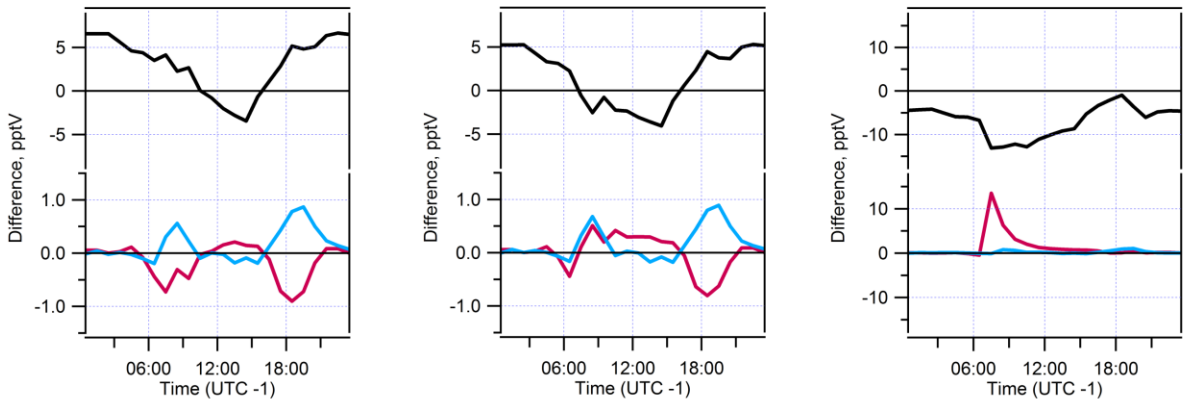

Figure 7. Sensitivity analysis of the effect of changing reactive uptake co-efficients (γ) of halogen nitrates , $XONO_2$ (X = Br, I), on NO_x (top) and XO (bottom) diurnal behaviour during summer months at CVO. The difference between measured and modelled values is plotted. Particulate nitrate photolysis is set at 10 times the rate of gaseous HNO_3.

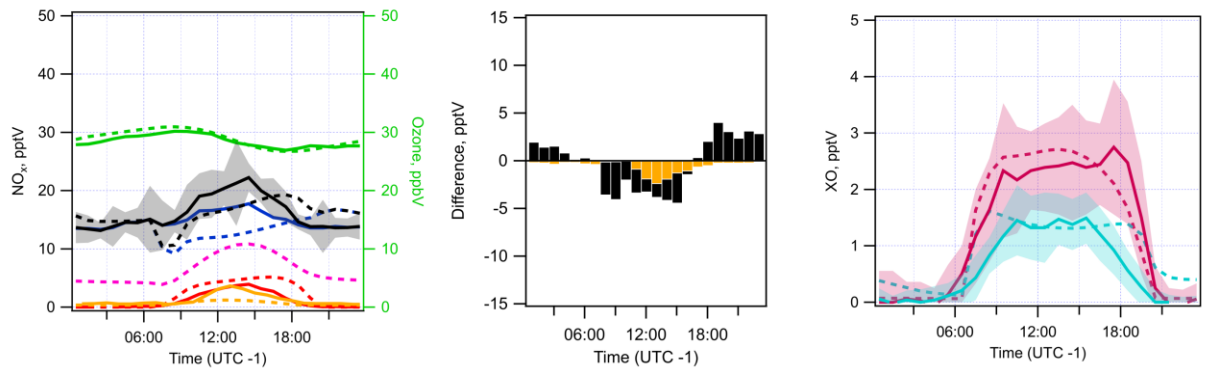

Figure 8. Left is the modelled NO_x and HONO diurnal cycle for the CVO site during summer months with the inclusion of night time HOI chemistry. Centre shows the difference between measured and modelled values of NO_x (black) and HONO (yellow). Right is the observed (adapted from Read et al., (2008)) and modelled IO and BrO. Observations are solid lines whilst modelled values are shown dashed. Shaded areas are standard error of the observation. O_3 – green; NO_x – black; NO_2 – blue; NO – red; HONO – yellow; PAN – pink; IO – turquoise; BrO – purple.

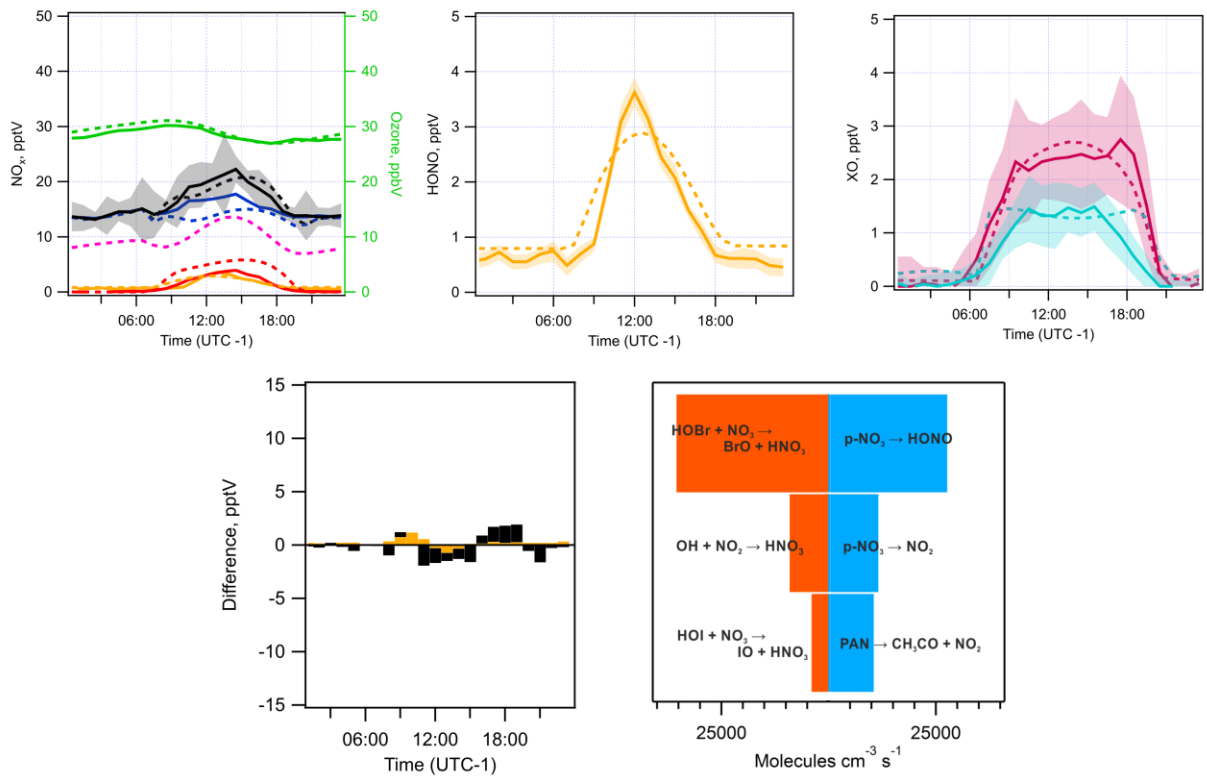

Figure 9. NO_x, O_3, HONO at CVO during summer months compared to model values when HOI and HOBr + NO_3 is included in the simulation. Top left: NO_x, O_3, HONO, and PAN diurnal cycles. Top middle: expanded view of modelled and measured HONO. Top right: observed (adapted from Read et al., (2008)) and modelled IO and BrO. Bottom left: difference between modelled and measured NO_x and HONO. Bottom right: the net production and loss analysis for NO_x in this simulation. O_3 – green; NO_x – black; NO_2 – blue; NO – red; HONO – yellow; PAN – pink; IO – turquoise; BrO – purple. Measured values are solid lines, modelled values are dashed.

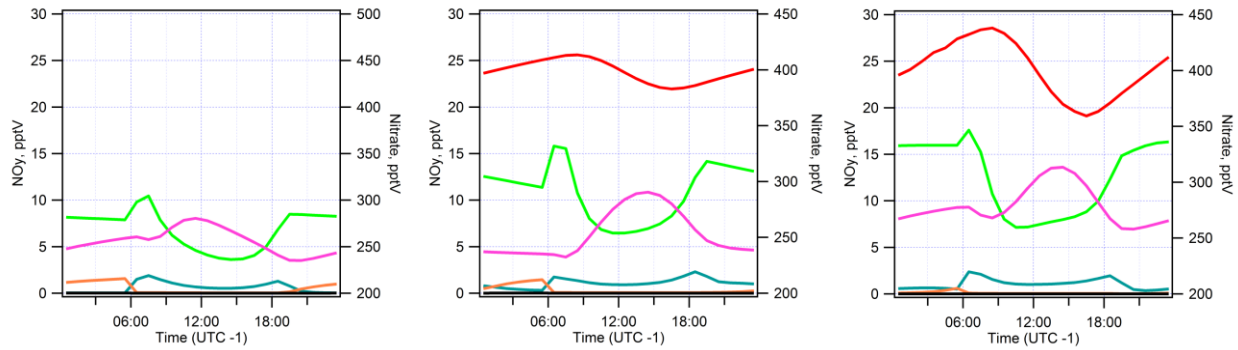

Figure 10. Shown are NO_y diurnals for the CVO site during summer months in the base scenario (left), with HOI + NO_3 chemistry included (centre), and with HOI & HOBr + NO_3 chemistry included (right). $BrONO_2$ = green, $IONO_2$ = teal, PAN = pink, NO_3 = orange, N_2O_5 = black, p-NO_3 - red.

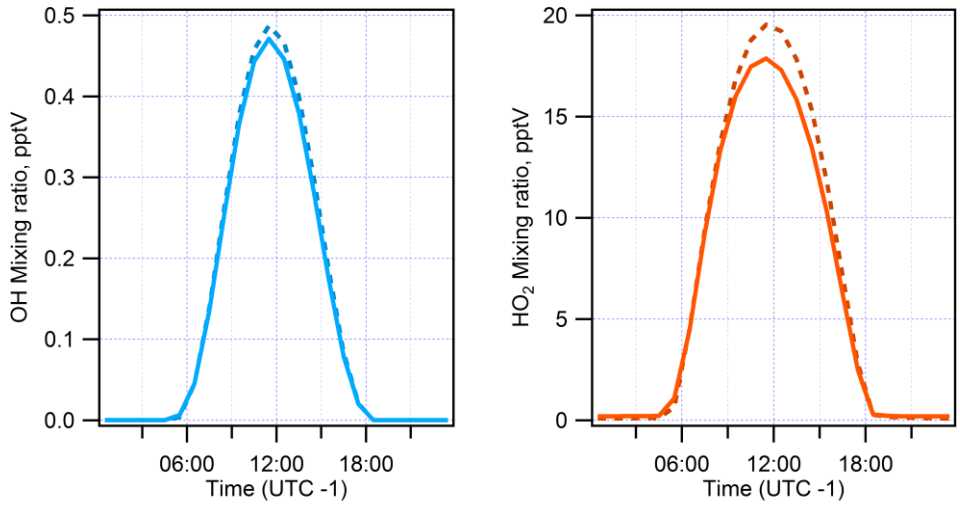

Figure 11. Modelled OH (left) and HO_2 (right) mixing ratios comparing the base case model where PAN decomposition is the dominant source of NO_x in the remote MBL (solid lines), with the final model where the dominant source of NO_x is particulate nitrate photolysis and HOX + NO_3 chemsitry is included (dashed lines).